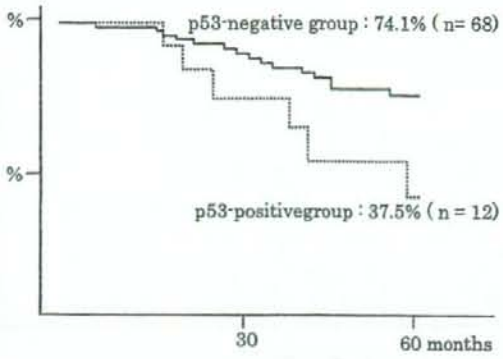

No. of patients at risk

	0M	12M	24M	36M	48M	60M
p53-negative (N=68)	68	67	63	58	54	53
p53-positve (N=12)	12	12	10	9	7	6

2. Survival curves for node negative patients with and without protein expression. *P* value = 0.022

variate analysis (Table 2). A five-year survival rate p53-negative and p53-positive patients are 59.7% l 23.9% respectively (P value is 0.0163. Fig. 1). In le-negative patients, overexpression of p53 protein l blood vessel invasion are prognostic factor. A e-year survival rate of p53-negative and p53- itive patients in node-negative patients are 74.1% l 37.5% respectively (*P* value is 0.022. Fig. 2). ltivariate analysis showed that only overexpres- n of p53 protein was an independent prognostic tor in node-negative lung adenocarcinoma ble 3).

Discussion

Our results in this study show that nuclear p53 erexpression is an independent prognostic factor in de-negative lung adenocarcinoma using immuno- tochemical staining. Furthermore, p53 protein erexpression correlates with lymphatic vessel asion.

p53 is an important molecule in tumorigenesis and ncer progression. The p53 gene is mutated in over lf of all human cancers, including lung cancer [12, ,19,20]. The functions of p53 gene have been own in recent numerous studies. In particular, mber of studies has been done about the field of carcinogenesis. p53 protein is stabilized when the cells are suffered several kinds of damage, which extend to DNA injury [10]. p53 then cause to DNA repair or apoptosis through activation or inactivation of down-stream genes. However, it is still unclear how p53 alteration contributes the prognosis of patients with cancer. Previous study has shown that p53 gene is involved in angiogenesis[21].

Gautam et.al. have also shown in their basic animal model that p53 gene delivery into cancer cells cause to suppress the distant metastasis thorough up-regulation of anti- angiogenic molecule and down- regulation of VEGF, which is known as major angiogenic molecules and is overexpressed in several type of cancer[22].The other side, Nakajima et al. have shown that p53 expression correlates with lymphatic vessel invasion and nodal metastasis in human esophageal cancer [23]. Our data also suggest that p53 protein overexpression in lung adenocarcinoma correlates with lymphatic vessels invasion. p53 alteration may play a roll for metastasis through

Table 3
Multivariate analysis for prognosis using Cox proportional hazard model

Factor	Coefficient	Standard error	*P* value
Total patients			
p53 protein	0.652	0.399	0.1025
N factor	1.272	0.327	0.0001
ly factor	0.514	0.344	0.1354
v factor	0.264	0.339	0.4367
Differentiation			
Well-Moderate	0.483	0.395	0.2219
Well-Poor	0.234	0.526	0.6569
T factor			
T1-T4	1.694	0.658	0.01
T2-T4	1.421	0.603	0.0185
T3-T4	1.179	0.708	0.0961
Node-negative patients			
Factor	Coefficient	Standard error	P value
p53 protein	1.11	0.551	0.0438
N factor	–	–	–
ly factor	0.422	0.542	0.4363
v factor	0.74	0.515	0.1503
Differentiation			
Well-Moderate	0.645	0.694	0.353
Well-Poor	0.013	0.815	0.9874
T factor			
T1-T4	2.243	1.279	0.079
T2-T4	1.101	1.253	0.3796
T3-T4	2.015	1.558	0.1959

angiogenesis and/or vessels invasion in lung adenocarcinoma at least in part. Further study including basic study should be needed to clarify the mechanism of p53 on metastasis.

In previous survival analysis, many report have shown that p53 protein overexpression and /or p53 gene mutation correlates with outcome in patients with lung cancer. More recently, several meta-analysis have shown that p53 protein overexpression is a prognostic factor at least in patients with lung adenocarcinoma [13]. Only a few reports have shown that p53 overexpression is one of the prognostic factor for node-negative lung cancer. Therefore, in node-negative patients, the prognostic value of p53 overexpression is still controversy. In node-negative status, nearly 40% of patients have recurrences after curative surgical treatment [3–5]. Definite and clinically useful prognostic factor is needed for those patients to predict a prognosis or to choose adequate adjuvant therapy after surgery.

In summary, our study suggests that p53 protein overexpression is an independent prognostic factor in patients with node-negative lung adenocarcinoma. The future study should be needed to confirm our findings using much sized number of patients and also using prospective study.

References

[1] J.D. Minna, J.A. Roth, A.F. Gazdar, Focus on lung cancer, Cancer Cell 1 (2002) 49–52.

[2] E. Steels, M. Paesmans, T. Berghmans, F. Branle, F. Lemaitre, C. Mascaux, et al., Role of p53 as a prognostic factor for survival in lung cancer: A systematic review of literature with a meta-analysis, Eur. Respir. J. 18 (2001) 705–719.

[3] H. Han, R.J. Landreneau, T.S. Santucci, M.Y. Tung, R.S. Machere, S.E. Shackney, et al., Prognostic value of immunohistochemical expressions of p53, HER-2/neu, and bcl-2 in stage I non-small-cell lung cancer, Hum. Pathol. 33 (2002) 105–110.

[4] J.C. Nesbitt, J.B. Putnam Jr., G.L. Walsh, J.A. Roth, C.F. Mountain, Survival in early-stage non-small cell lung cancer, Ann. Thorac. Surg. 60 (1995) 466–472.

[5] H. Wada, F. Tanaka, K. Yanagihara, T. Ariyasu, T. Fukuse, H. Yokomise, et al., Time trends and survival after operations for primary lung cancer from 1976 through 1990, J. Thorac. Cardiovasc. Surg. 112 (1996) 349–355.

[6] M. Adachi, T. Taki, M. Higashiyama, N. Kohno, H. Inufusa, M. Miyake, Significance of integrin alpha5 gene expression as a prognostic factor in node-negative non-small cell lung cancer, Clin. Cancer Res. 6 (2000) 96–101.

[7] J.M. Siegfried, L.A. Weissfeld, J.D. Luketich, R.J. Weyant, C. T. Gubish, R.J. Landreneau, The clinical significance of hepatocyte growth factor for non-small cell lung cancer, Ann. Thorac. Surg. 66 (1998) 1915–1918.

[8] M.I. Koukourakis, A. Giatromanolaki, K.J. O'Byrne, M. Comley, R.M. Whitehouse, D.C. Talbot, et al., Platelet-derived endothelial cell growth factor expression correlates with tumour angiogenesis and prognosis in non-small-cell lung cancer, Br. J. Cancer 75 (1997) 477–481.

[9] A. Giatromanolaki, M.I. Koukourakis, K. O'Byrne, L. Kaklamanis, C. Dicoglou, E. Trichia, et al., Non-small cell lung cancer: c-erbB-2 overexpression correlates with low angiogenesis and poor prognosis, Anticancer Res. 16 (1996) 3819–3825.

[10] J. Gu, L. Zhang, S.G. Swisher, J. Liu, J.A. Roth, B. Fang, Induction of p53-regulated genes in lung cancer cells: implications of the mechanism for adenoviral p53-mediated apoptosis, Oncogene 23 (2004) 1300–1307.

[11] V.G. Gorgoulis, P.V. Zacharatos, E. Manolis, J.A. Ikonomopoulos, A. Damalas, C. Lamprinopoulos, et al., Effects of p53 mutants derived from lung carcinomas on the p53-responsive element (p53RE) of the MDM2 gene, Br. J. Cancer 77 (1998) 374–384.

[12] K. Gemba, H. Ueoka, K. Kiura, M. Tabata, M. Harada, Immunohistochemical detection of mutant p53 protein in small-cell lung cancer: relationship to treatment outcome, Lung Cancer 29 (2000) 23–31.

[13] T. Mitsudomi, N. Hamajima, M. Ogawa, T. Takahashi, Prognostic significance of p53 alterations in patients with non-small cell lung cancer: a meta-analysis, Clin. Cancer Res. 6 (2000) 4055–4063.

[14] C.C. Harris, Structure and function of the p53 tumor suppressor gene: clues for rational cancer therapeutic strategies, J. Natl Cancer Inst. 88 (1996) 1442–1455.

[15] P. Dalquen, G. Sauter, J. Torhorst, E. Schultheiss, P. Jordan, S. Lehmann, et al., Nuclear p53 overexpression is an independent prognostic parameter in node-negative non-small cell lung carcinoma, J. Pathol. 178 (1996) 53–58.

[16] J.S. Lee, A. Yoon, S.K. Kalapurakal, J.Y. Ro, J.J. Lee, N. Tu, et al., Expression of p53 oncoprotein in non-small-cell lung cancer: a favorable prognostic factor, J. Clin. Oncol. 13 (1995) 1893–1903.

[17] S. Haga, M. Nakayama, K. Tatsumi, M. Maeda, S. Imai, S. Umesako, et al., Overexpression of the p53 gene product in canine mammary tumors, Oncol. Rep. 8 (2001) 1215–1219.

[18] D. Dworakowska, S. Gozdz, E. Jassem, A. Badzio, G. Kobierska, A. Urbaniak, et al., Prognostic relevance of proliferating cell nuclear antigen and p53 expression in non-small cell lung cancer, Lung Cancer 35 (2002) 35–41.

] M. Hollstein, D. Sidransky, B. Vogelstein, C.C. Harris, p53 mutations in human cancers, Science 253 (1991) 49–53.
] A.J. Levine, p53, the cellular gatekeeper for growth and division, Cell 88 (1997) 323–331.
] A. Yuan, C.J. Yu, K.T. Luh, S.H. Kuo, Y.C. Lee, P.C. Yang, Aberrant p53 expression correlates with expression of vascular endothelial growth factor mRNA and interleukin-8 mRNA and neoangiogenesis in non-small-cell lung cancer, J. Clin. Oncol. 20 (2002) 900–910.
[22] A. Gautam, C.L. Densmore, S. Melton, E. Golunski, J.C. Waldrep, Aerosol delivery of PEI-p53 complexes inhibits B16-F10 lung metastases through regulation of angiogenesis, Cancer Gene Ther. 9 (2002) 28–36.
[23] Y. Nakajima, K. Nagai, S. Miyake, K. Ohashi, T. Kawano, T. Iwai, Evaluation of an indicator for lymph node metastasis of esophageal squamous cell carcinoma invading the submucosal layer, Jpn. J. Cancer Res. 93 (2002) 305–312.

British Journal of Cancer (2006) 95, 601 – 606

www.bjcancer.com

NK105, a paclitaxel-incorporating micellar nanoparticle, is a more potent radiosensitising agent compared to free paclitaxel

T Negishi[1], F Koizumi[1], H Uchino[2], J Kuroda[1], T Kawaguchi[3], S Naito[2] and Y Matsumura[*,1]

[1]Investigative Treatment Division, Research Center for Innovative Oncology, National Cancer Center Hospital East, 6-5-1 Kashiwanoha, Kashiwa, Chiba 277-8577, Japan; [2]Department of Urology, Graduate School of Medical Sciences, Kyushu University, 3-1-1 Maidashi, Higashi-ku, Fukuoka, Fukuoka 812-8582, Japan; [3]Department of Anatomy and Histology, Fukushima Medical University School of Medicine, 1-Hikariga-oka, Fukushima, Fukushima 960-1247, Japan

NK105 is a micellar nanoparticle formulation designed to enhance the delivery of paclitaxel (PTX) to solid tumours. It has been reported to exert antitumour activity *in vivo* and to have reduced neurotoxicity as compared to that of free PTX. The purpose of this study was to investigate the radiosensitising effect of NK105 in comparison with that of PTX. Lewis lung carcinoma (LLC)-bearing mice were administered a single intravenous (i.v.) injection of PTX or NK105; 24 h after the drug administration, a proportion of the mice received radiation to the tumour site or lung fields. Then, the antitumour activity and lung toxicity were evaluated. In one subset of mice, the tumours were excised and specimens were prepared for analysis of the cell cycle distribution by flow cytometry. Combined NK105 treatment with radiation yielded significant superior antitumour activity as compared to combined PTX treatment with radiation ($P=0.0277$). On the other hand, a histopathological study of lung sections revealed no significant difference in histopathological changes between mice treated with PTX and radiation and those treated with NK105 and radiation. Flow-cytometric analysis showed that NK105-treated LLC tumour cells showed more severe arrest at the G2/M phase as compared to PTX-treated tumour cells. The superior radiosensitising activity of NK105 was thus considered to be attributable to the more severe cell cycle arrest at the G2/M phase induced by NK105 as compared to that induced by free PTX. The present study results suggest that further clinical trials are warranted to determine the efficacy and feasibility of combined NK105 therapy with radiation.
British Journal of Cancer (2006) **95**, 601–606. doi:10.1038/sj.bjc.6603311 www.bjcancer.com
Published online 8 August 2006

Keywords: paclitaxel; NK105; radiosensitiser; polymer micelle; drug delivery system

Paclitaxel (PTX) has been demonstrated to be one of the most effective anticancer agents available at present (Carney, 1996; Khayat *et al*, 2000). Besides its antitumour activity, its ability to induce radiosensitisation has been reported both *in vitro* (Tishler *et al*, 1992; Choy *et al*, 1993; Lokeshwar *et al*, 1995; Rodriguez *et al*, 1995) and *in vivo* (Milas *et al*, 1994, 1995; Cividalli *et al*, 1998) this effect has been attributed to its effect of stabilising microtubules and inducing cell cycle arrest at the G2/M phase, the most radiosensitive phase of the cell cycle (Terasima and Tolmach, 1963; Sinclair and Morton, 1966). As several clinical studies have demonstrated the efficacy of PTX-based chemotherapy combined with radiotherapy, the combined modality is considered to be a potentially important treatment option for lung and breast cancer (Choy *et al*, 1998a, b, 2000; Dowell *et al*, 1999; Formenti *et al*, 2003; Kao *et al*, 2005).

The adverse effects of radiation, namely, lung toxicities in patients with breast or lung cancer treated by thoracic radiation, are of great concern, and may be dose limiting or even have a negative impact on the quality of life of the patients, even though radiation is an efficient treatment option. Lung toxicities often result in lung fibrosis, necessitating change of the treatment method and causing much distress or even death of the patients (Penney and Rubin, 1977; Early Breast Cancer Trialists' Collaborative Group, 2000; Lind *et al*, 2002). Some clinical trials actually reported an increased incidence of pneumonitis following combined PTX therapy with radiation in patients with breast or lung cancer (Taghian *et al*, 2001; Hanna *et al*, 2002; Chen and Okunieff, 2004).

Although widely used, PTX itself has several adverse effects, such as peripheral sensory neuropathy (Rowinsky *et al*, 1993; Rowinsky and Donehower, 1995), and its poor solubility in water is also associated with such effects as anaphylaxis and other severe hypersensitivity reactions attributable to Cremophor EL and ethanol, which are essential for solubilising PTX (Weiss *et al*, 1990; Rowinsky and Donehower, 1995). In order to overcome these problems, we prepared a new formulation, NK105, which is a PTX-incorporating polymeric micellar nanoparticle (85 nm in size) (Hamaguchi *et al*, 2005). NK105 is formed by facilitating the self-association of amphiphilic block copolymers constructed using polyethylene glycol (PEG) as the hydrophilic segment and modified polyaspartate as the hydrophobic segment in an aqueous medium. Owing to the PEG constituting the outer shell of the micelles, NK105 is soluble in water. In addition, PEG also confers a stealth property to the formulation, that allows the micellar drug preparation to be less avidly taken up by the reticuloendothelial

*Correspondence: Dr Y Matsumura; E-mail: yhmatsum@east.ncc.go.jp
Revised 5 June 2006; accepted 11 July 2006; published online 8 August 2006

system (RES) and to be retained in the circulation for a longer period of time (Klibanov *et al*, 1990, 1991; Allen, 1994; Gabizon *et al*, 1996). The prolonged circulation time and the ability of NK105 to extravasate through the leaky tumour vasculature (i.e., the EPR (enhanced permeability and retention) effect) causes accumulation of PTX in tumour tissues (Matsumura and Maeda, 1986; Maeda and Matsumura, 1989). We previously demonstrated that NK105 is associated with reduced neurotoxicity and also exerts more potent antitumour activity on human cancer xenograft, as compared to free PTX. In addition, because of its solubility in water, it is expected that the incidence of anaphylaxis and hypersensitivity reactions attributable to Cremophor EL and ethanol may also be reduced with NK105. A clinical trial of NK105 is now under way.

In this context, it is expected that the use of NK105 in place of PTX in combination with radiation may also yield superior results, because of the more potent antitumour activity of this drug as compared to that of free PTX. In this study, we evaluated the antitumour activity and severity of lung fibrosis induced by PTX and NK105 administered in combination with thoracic radiation, to examine whether combined NK105 chemotherapy with radiation would be an acceptable or useful treatment modality.

MATERIALS AND METHODS

Mice

Eight-week-old female C57BL/6J mice were purchased from Charles River Japan Inc. (Kanagawa, Japan). All the animal procedures were performed in compliance with the guidelines for the care and use of experimental animals, drawn up by the Committee for Animal Experimentation of the National Cancer Center; these guidelines meet the ethical standards required by law and also comply with the guidelines for the use of experimental animals in Japan.

PTX and NK105

Paclitaxel was purchased from Merican Corp. (Tokyo, Japan). NK105 is a PTX-incorporating 'core-shell-type' polymeric micellar nanoparticle formulation that was prepared by a previously reported procedure (Hamaguchi *et al*, 2005). Briefly, polymeric micellar particles were formed by facilitating the self-association of amphiphilic block copolymers in an aqueous medium. The polymer of NK105 was constructed using PEG as the hydrophilic segment and modified polyaspartate as the hydrophobic segment. The carboxylic groups of the polyaspartate block were modified by the esterification reaction with 4-phenyl-1-butanol, resulting in conversion of half of the groups to 4-phenyl-1-butanolate. Molecular weight of the polymers was determined to be approximately 2000 (PEG block: 12 000; moditied polyaspartate block: 8000).

Via the self-association process, PTX was incorporated into the inner core of the micelle system by physical entrapment through hydrophobic interactions between the drug and specifically well-designed block copolymers for PTX. NK105 was obtained as a freeze-dried formulation and contained ca.23% (WW^{-1}) of PTX. Finally, NK105, PTX-incorporating polymeric micellar nanoparticle formulation with a single and narrow size distribution, was obtained. The weight-average diameter of the nanoparticles was approximately 85 nm ranging from 20 to 430 nm.

Irradiation

The mice were anesthetised by intraperitoneal (i.p.) injection of nembutal (75 mg kg^{-1}) and placed on the stage for irradiation. The whole thorax or subcutaneous (s.c.) tumours of the thigh were irradiated using a Faxitron cabinet X-ray system model CP-160 by 100 kV X-rays from a linear accelerator, at a dose rate of 2 Gy min^{-1}. Totally 12 Gy was irradiated to each mouse. The whole body except irradiated parts, lung field or tumour lesion, were shielded with specially designed lead blocks.

Flow cytometry

At 24 h after the injection of PTX or NK105 into the Lewis lung carcinoma (LLC) tumour-bearing C57BL/6j mice, the tumours were excised, minced in PBS, and fixed in 70% ethanol at 4°C for 48 h. After being fixed, the tumours were digested with 0.04% pepsin (Sigma chemical co., St Louis, MO, USA) in 0.1 N HCl for 60 min at 37°C in a shaking bath for preparing single-nuclei suspensions. The nuclei were then centrifuged, washed twice with PBS, and stained with 40 $\mu g\,ml^{-1}$ of propidium iodide (Molecular Probes, OR, USA) in the presence of 100 $\mu g\,ml^{-1}$ RNase in 1 ml PBS for 30 min at 37°C. The stained nuclei were analysed with a B-D FACSCalibur (BD Biosciences, San Jose, CA, USA). The cell cycle distribution was analysed using the Modfit program (Verity Software House Inc., Topsham, ME, USA).

Evaluation of the antitumour activity

For this experiment, 3×10^6 LLC cells were inoculated s.c. into the right thighs of mice. The tumour volume was calculated using the formula, tumour volume (mm^3) = $a \times b^2/2$ (a = longest tumour diameter, b = shortest tumour diameter). When the tumour volume reached approximately 100 mm^3 on day 14 after the tumour inoculation, the mice were randomly allocated to test groups of about four or five mice each, and started the treatment on the same day. There were six test groups, as follows: untreated control, PTX treatment alone, NK105 treatment alone, radiation alone, combined PTX treatment with radiation, and combined with NK105 treatment with radiation.

In the groups receiving PTX or NK105, the mice were administered a single intravenous (i.v). injection of PTX or NK105 at the dose of 45 mg kg^{-1}; 24 h after the drugs were administered, the tumour sites of the mice in the groups scheduled to receive radiation were irradiated.

The antitumour activity of each treatment regimen was evaluated by measuring the tumour volume. Tumour volume and body weight was measured every 3 days.

Evaluation of lung toxicity

The severity of lung toxicity was evaluated histologically in the following test groups; untreated control ($n = 6$), radiation treatment alone ($n = 6$), combined PTX treatment with radiation ($n = 9$), and combined NK105 treatment with radiation ($n = 10$). Mice were administered a single i.v. injection of PTX or NK105 at the dose of 45 mg kg^{-1}; 24 h after the drugs were administered, the thorax of the mice in the groups scheduled to receive radiation was irradiated. All the mice were killed 36 weeks after the drug administration. At the time of the killing, the lungs were removed, and the right lungs were fixed in 10% buffered formalin for 24 h, then embedded in paraffin. The lungs were inflated at 20 cm water pressure by intratracheal infusion of 10% buffered formalin before fixation. Sections (5 μm- thick) were stained with haematoxylin and eosin (H&E) and observed under the light microscope. The severity of the pulmonary fibrosis was assessed based on Ashcroft's scoring system (Ashcroft *et al*, 1988). Briefly, all the fields of each lung section were scanned under a Leica microscope at a magnification of × 100, then each field was visually graded from 0 (normal lung) to 8 (total fibrotic obliteration of the field). The mean grades obtained for all of the fields was then calculated as the visual fibrotic score.

Immunohistochemistry

The lung sections were deparaffinised and rehydrated, then microwaved in 0.01 M sodium citrate buffer for 15 min at 90°C to retrieve epitopes, and cooled at room temperature. An endogenous peroxidase blocking solution of 3% hydrogen peroxide was applied for 20 min at room temperature. After blocking the nonspecific binding sites with 2% normal goat serum, the sections were incubated with rabbit anti-mouse collagen III immunoglobulin G (IgG) (Chemicon International, Temecula, CA, USA) overnight at 4°C. The sections were then washed with PBS, followed by the addition of biotin-conjugated goat anti-rabbit IgG (Vector Laboratories Inc., Burlingame, CA, USA) and incubation for 30 min at room temperature. The sections were then washed and incubated with horseradish-peroxidase-conjugated avidin–biotin complex (Vector Laboratories Inc., Burlingame, CA, USA) at room temperature for 30 min, in accordance with the manufacturer's instructions (Vector Laboratories Inc.). The immunoreactions were visualised using 3,3′-diaminobenzidine as the substrate and counterstaining with haematoxylin.

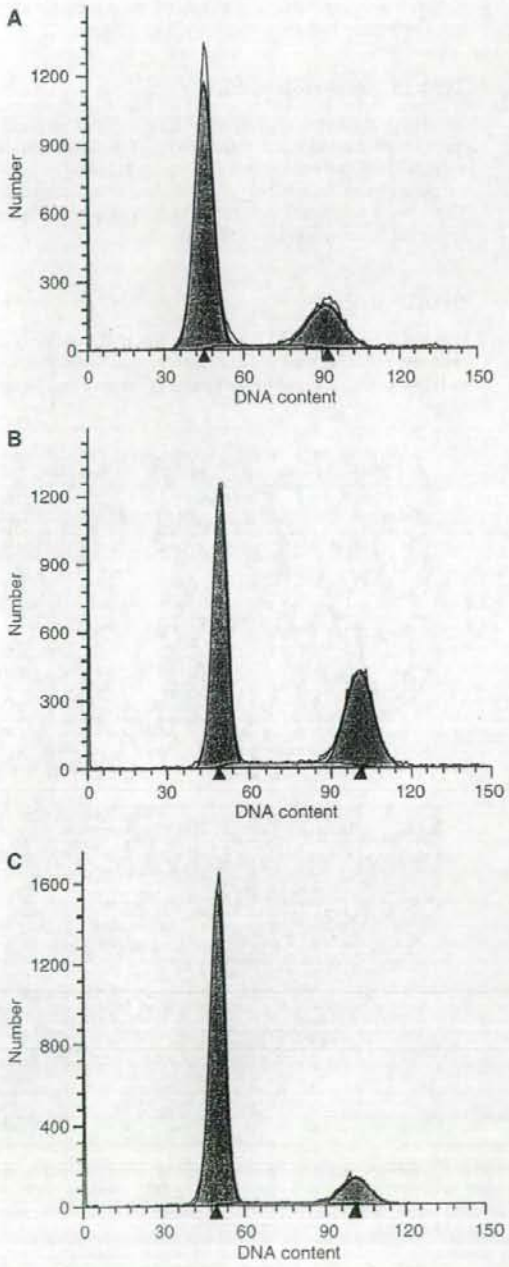

Figure 1 Cell cycle analysis. Cell cycle analysis of LLC tumour cells 24 h after PTX (**A**) or NK105 administration (**B**). Untreated control cells are shown in (**C**).

Statistical analysis

Date were expressed the mean ± s.d. Differences between the test groups were analysed by Student's *t*-test. We used Stat View (SAS Institute Inc.) statistical software. A value of $P<0.05$ was considered statistically significant.

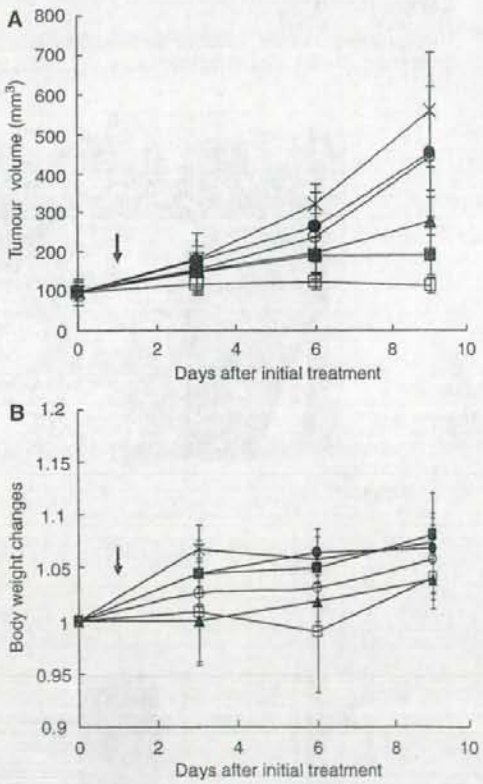

Figure 2 Antitumour activity. Changes in the LLC tumour growth rates in the mice. (**A**) Mice receiving TXL-alone (●), NK105-alone (○), combined treatment with PTX and radiation (■), and combined treatment with NK105 and radiation (□) were administered a single i.v. injection of PTX or NK105 at the dose 45 mg kg^{-1} on day 14 after the tumour inoculation (= on day 0 after the initial treatment). After 24 h the drugs were administered, the mice in the radiation-alone (Δ) and the combined-treatment groups were irradiated (arrow). Mice in the control group (×) were given no treatment. (**B**) Changes in the relative body weight. Data were derived from the same mice as those used in the present study.

RESULTS

Cell cycle analysis

At 24 h after the administration of PTX or NK105 to the LLC-tumour-bearing mice, severe cell cycle arrest at the G2/M phase was observed in the tumour cells treated with the drugs as compared with that in the control (no drug treatment) (Figure 1C). There was a tendency towards the NK105-treated LLC tumour cells (Figure 1B) showing more severe arrest at the G2/M phase than the PTX-treated cells (Figure 1A).

Antitumour activity

Decreased tumour growth rates of the LLC tumours were observed in the mice of the radiation alone, combined PTX with radiation, and combined NK105 with radiation groups. No antitumour activity was observed following treatment with either PTX or NK105 alone, because LLC is primarily a PTX-resistant tumour. Combined NK105 therapy with radiation yielded superior antitumour activity as compared to both radiation alone ($P=0.0047$) and combined PTX therapy with radiation ($P=0.0277$) on the day 9 after the treatment initiation (Figure 2A). No significant differences in body weight changes were noted among the groups tested (Figure 2B).

Lung toxicities

Histopathological examination of the lung sections of all the mice receiving radiation showed inflammatory cell infiltration, appearance of intra-alveolar macrophages, and destruction of the alveolar architecture. Major portions of the alveolar septa in the lung sections prepared from the irradiated mice showed slight thickening, although no massive structural destruction was observed (Figure 3A). On the other hand, the lung sections prepared from the control nonirradiated group showed no significant histopathological changes (Figure 3B). Ashcroft's fibrosis scores in the groups of mice that received radiation ranged from 0.975 to 1.426, with no significant differences among the groups. The score in the control group was nearly zero. In the groups receiving radiation, the severity of lung fibrosis differed significantly among the mice within the same groups, as did the Ashcroft's scores, that is, the s.d. of the Ashcroft's scores in the mice receiving radiation was very high (Figure 3C).

Type III collagen deposition

Immunohistochemical analysis of lung sections prepared from the mice receiving radiation revealed significant collagen deposition, especially in the subpleural regions, while that of lung sections prepared from the control group showed little collagen deposition. There were no significant differences among the different groups receiving radiation (Figure 3D).

DISCUSSION

It is well known that PTX enhances the radiosensitivity of tumour cells by inducing cell cycle arrest at the G2/M phase, the most radiosensitive phase of the cell cycle (Terasima and Tolmach, 1963;

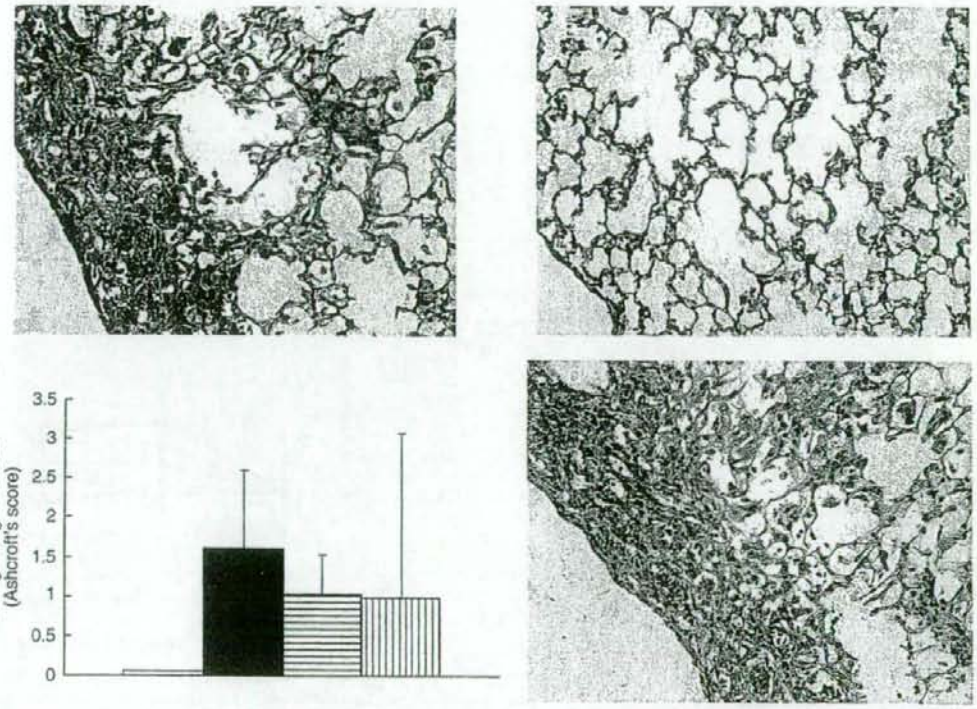

Figure 3 H&E staining of the lungs of C57BL/6J mice surviving 36 weeks after the thoracic radiation (**A**) and sham radiation (**B**). (**C**) Semiquantitative analyses to estimate the severity of pulmonary fibrosis in the mice receiving sham radiation (□), thoracic radiation alone (■), combined PTX with radiation (▤), and combined NK105 with radiation (▥). H&E- stained lung tissue sections were assessed to estimate the severity of pulmonary fibrosis by visual grading of fibrosis (Ashcroft's score). Collagen III staining of the irradiated lungs of mice (**D**).

Sinclair and Morton, 1966). Many reports have confirmed the radiosensitising effect of PTX in different cell lines (Tishler *et al*, 1992; Choy *et al*, 1993; Lokeshwar *et al*, 1995; Rodriguez *et al*, 1995), *in vivo* experiments (Milas *et al*, 1994, 1995; Cividalli *et al*, 1998), and in several clinical trials of combined PTX with radiation therapy according to different schedules (Dillman *et al*, 1990; Arriagada *et al*, 1991; Morton *et al*, 1991; Furuse *et al*, 1999; Sause *et al*, 2000; Chen *et al*, 2003). Chen *et al* (2003) examined the optimal timing of PTX treatment and irradiation in relation to the cell cycle, and recommended that radiation be given at least 5 h after PTX administration, because G2/M arrest of a lung cancer cell line was shown to start at 4 h after PTX treatment and to last for 44 h.

In our experimental model to evaluate the antitumour activity, the tumours were irradiated 24 h after a single i.v. injection of PTX or NK105. No significant increase in the antitumour activity as compared with that in the control (no treatment) was observed following a single i.v. injection of either PTX or NK105 at the dose of 45 mg kg^{-1}; LLC tumours are known to be primarily resistant to PTX. In fact, the IC_{50} of PTX against an LLC tumour cell line was shown to be 84.1 nM, which is about 10-fold higher than that of NK105 against various cancer cell lines tested in our previous work (Hamaguchi *et al*, 2005). Combined NK105 therapy with radiation yielded superior antitumour activity as compared with radiation alone or combined PTX therapy with radiation. This result suggests that NK105 has a more potent radiosensitising effect than PTX. In our study, there was a tendency towards NK105-treated LLC tumour cells showing more severe arrest at the G2/M phase as compared to PTX-treated cells at 24 h after the injection of the drugs, the timing of the radiation treatment, probably because NK105 allows a higher concentration of PTX to be maintained in the tumour than conventional PTX (Hamaguchi *et al*, 2005). We suppose that this is the reason why NK105 exerted more potent radiosensitising activity than PTX.

Next, we were concerned about the adverse effects of combined NK105 therapy with radiation. New micellar drugs are designed based on the idea that DDS can accumulate in the tumour selectively, while showing reduced distribution in normal tissues. We demonstrated that the incorporation of cisplatin into micelles significantly reduced the nephrotoxicity and neurotoxicity of cisplatin (Uchino *et al*, 2005). However, it was also shown that micelle- incorporated cisplatin caused transient liver dysfunction because it was trapped more avidly by the RES as compared to free cisplatin, even though the PEG of the outer shell of the micelle confers the so-called stealth effect.

In this study, our examination of the lung sections of mice treated with NK105 and radiation revealed that the histopathological changes such as inflammatory cell infiltration, appearance of intra-alveolar macrophages, and destruction of the alveolar architecture were induced by thoracic radiation and not by the accumulation of NK105 in the lung. There were no significant differences in the histopathological changes observed among the mice treated by NK105 and radiation and mice treated by radiation alone or PTX with radiation. The severity of lung fibrosis did not differ significantly among the test groups either. Although some clinical trials reported an increased incidence of pneumonitis and esophagitis following combined PTX therapy with radiation (Taghian *et al*, 2001; Hanna *et al*, 2002; Chen and Okunieff, 2004), others reported no influence on the incidence of such adverse effects (Ellerbroek *et al*, 2003; Yu *et al*, 2003). Several clinical trials and *in vivo* experiments have discussed the subject, however, no definitive conclusion has been arrived at (Mason *et al*, 1995; Choy *et al*, 1998; Yu *et al*, 2004; Kao *et al*, 2005). In our study, in regard to the incidence of esophagitis, there were no significant differences in the histopathological changes observed in the esophageal sections at one week after the treatment among the test groups (data not shown).

In conclusion, we demonstrated that combined NK105 chemotherapy with radiation exerts significant antitumour activity. Furthermore, the lung toxicity of this combined treatment modality was also acceptable as compared with that observed following radiation alone or combined PTX therapy with radiation. However, further studies are necessary to determine the effectiveness of NK105 in terms of its radiosensitising effect.

ACKNOWLEDGEMENTS

We thank Drs K Sugiyama and K Tsuchihara for their scientific advice and Mrs C Kanai and Mrs N Mie for their technical assistance. We are also grateful to Mrs K Shiina for her secretarial assistance. This work was supported by a Grant-in-Aid from the Ministry of Health, Labor and Welfare of Japan (Y Matsumura) and a Grant-in-Aid for Scientific Research on Priority Areas from the Ministry of Education, Culture, Sports, Science and Technology (Y Matsumura).

REFERENCES

Allen TM (1994) Long-circulating (sterically stabilized) liposomes for targeted drug delivery. *Trends Pharmacol Sci* **15**: 215–220

Arriagada R, Le Chevalier T, Quoix E, Ruffie P, de Cremoux H, Douillard JY, Tarayre M, Pignon JP, Laplanche A (1991) ASTRO (American Society for Therapeutic Radiology and Oncology) plenary: Effect of chemotherapy on locally advanced non-small cell lung carcinoma: a randomized study of 353 patients. GETCB (Groupe d'Etude et Traitement des Cancers Bronchiques), FNCLCC (Federation Nationale des Centres de Lutte contre le Cancer) and the CEBI trialists. *Int J Radiat Oncol Biol Phys* **20**: 1183–1190

Ashcroft T, Simpson JM, Timbrell V (1988) Simple method of estimating severity of pulmonary fibrosis on a numerical scale. *J Clin Pathol* **41**: 467–470

Carney DN (1996) Chemotherapy in the management of patients with inoperable non-small cell lung cancer. *Semin Oncol* **23**: 71–75

Chen Y, Okunieff P (2004) Radiation and third-generation chemotherapy. *Hematol Oncol Clin North Am* **18**: 55–80

Chen Y, Pandya K, Keng PC, Johnstone D, Li J, Lee YJ, Smudzin T, Okunieff P (2003) Phase I/II clinical study of pulsed paclitaxel radiosensitization for thoracic malignancy: a therapeutic approach on the basis of preclinical research of human cancer cell lines. *Clin Cancer Res* **9**: 969–975

Choy H, Akerley W, Safran H, Graziano S, Chung C, Williams T, Cole B, Kennedy T (1998a) Multiinstitutional phase II trial of paclitaxel, carboplatin, and concurrent radiation therapy for locally advanced non-small-cell lung cancer. *J Clin Oncol* **16**: 3316–3322

Choy H, Devore III RF, Hande KR, Porter LL, Rosenblatt P, Yunus F, Schlabach L, Smith C, Shyr Y, Johnson DH (2000) A phase II study of paclitaxel, carboplatin, and hyperfractionated radiation therapy for locally advanced inoperable non-small-cell lung cancer (a Vanderbilt Cancer Center Affiliate Network Study). *Int J Radiat Oncol Biol Phys* **47**: 931–937

Choy H, Rodriguez FF, Koester S, Hilsenbeck S, Von Hoff DD (1993) Investigation of taxol as a potential radiation sensitizer. *Cancer* **71**: 3774–3778

Choy H, Safran H, Akerley W, Graziano SL, Bogart JA, Cole BF (1998b) Phase II trial of weekly paclitaxel and concurrent radiation therapy for locally advanced non-small cell lung cancer. *Clin Cancer Res* **4**: 1931–1936

Cividalli A, Arcangeli G, Cruciani G, Livdi E, Cordelli E, Danesi DT (1998) Enhancement of radiation response by paclitaxel in mice according to different treatment schedules. *Int J Radiat Oncol Biol Phys* **40**: 1163–1170

Dillman RO, Seagren SL, Propert KJ, Guerra J, Eaton WL, Perry MC, Carey RW, Frei III EF, Green MR (1990) A randomized trial of induction

chemotherapy plus high-dose radiation *vs* radiation alone in stage III non-small-cell lung cancer. *N Engl J Med* 323: 940–945

Dowell JE, Sinard R, Yardley DA, Aviles V, Machtay M, Weber RS, Weinstein GS, Chalian AA, Carbone DP, Rosenthal DI (1999) Seven-week continuous-infusion paclitaxel concurrent with radiation therapy for locally advanced non-small cell lung and head and neck cancers. *Semin Radiat Oncol* 9: 97–101

Early Breast Cancer Trialists' Collaborative Group (2000) Favourable and unfavourable effects on long-term survival of radiotherapy for early breast cancer: an overview of the randomised trials. Early Breast Cancer Trialists' Collaborative Group. *Lancet* 355: 1757–1770

Ellerbroek N, Martino S, Mautner B, Tao ML, Rose C, Botnick L (2003) Breast-conserving therapy with adjuvant paclitaxel and radiation therapy: feasibility of concurrent treatment. *Breast J* 9: 74–78

Formenti SC, Volm M, Skinner KA, Spicer D, Cohen D, Perez E, Bettini AC, Groshen S, Gee C, Florentine B, Press M, Danenberg P, Muggia F (2003) Preoperative twice-weekly paclitaxel with concurrent radiation therapy followed by surgery and postoperative doxorubicin-based chemotherapy in locally advanced breast cancer: a phase I/II trial. *J Clin Oncol* 21: 864–870

Furuse K, Fukuoka M, Kawahara M, Nishikawa H, Takada Y, Kudoh S, Katagami N, Ariyoshi Y (1999) Phase III study of concurrent *vs* sequential thoracic radiotherapy in combination with mitomycin, vindesine, and cisplatin in unresectable stage III non-small-cell lung cancer. *J Clin Oncol* 17: 2692–2699

Gabizon A, Chemla M, Tzemach D, Horowitz AT, Goren D (1996) Liposome longevity and stability in circulation: effects on the *in vivo* delivery to tumors and therapeutic efficacy of encapsulated anthracyclines. *J Drug Target* 3: 391–398

Hamaguchi T, Matsumura Y, Suzuki M, Shimizu K, Goda R, Nakamura I, Nakatomi I, Yokoyama M, Kataoka K, Kakizoe T (2005) NK105, a paclitaxel-incorporating micellar nanoparticle formulation, can extend *in vivo* antitumour activity and reduce the neurotoxicity of paclitaxel. *Br J Cancer* 92: 1240–1246

Hanna YM, Baglan KL, Stromberg JS, Vicini FA, A Decker D (2002) Acute and subacute toxicity associated with concurrent adjuvant radiation therapy and paclitaxel in primary breast cancer therapy. *Breast J* 8: 149–153

Kao J, Conzen SD, Jaskowiak NT, Song DH, Recant W, Singh R, Masters GA, Fleming GF, Heimann R (2005) Concomitant radiation therapy and paclitaxel for unresectable locally advanced breast cancer: results from two consecutive phase I/II trials. *Int J Radiat Oncol Biol Phys* 61: 1045–1053

Khayat D, Antoine EC, Coeffic D (2000) Taxol in the management of cancers of the breast and the ovary. *Cancer Invest* 18: 242–260

Klibanov AL, Maruyama K, Beckerleg AM, Torchilin VP, Huang L (1991) Activity of amphipathic poly(ethylene glycol) 5000 to prolong the circulation time of liposomes depends on the liposome size and is unfavorable for immunoliposome binding to target. *Biochim Biophys Acta* 1062: 142–148

Klibanov AL, Maruyama K, Torchilin VP, Huang L (1990) Amphipathic polyethyleneglycols effectively prolong the circulation time of liposomes. *FEBS Lett* 268: 235–237

Lind PA, Marks LB, Hardenbergh PH, Clough R, Fan M, Hollis D, Hernando ML, Lucas D, Piepgrass A, Prosnitz LR (2002) Technical factors associated with radiation pneumonitis after local +/− regional radiation therapy for breast cancer. *Int J Radiat Oncol Biol Phys* 52: 137–143

Lokeshwar BL, Ferrell SM, Block NL (1995) Enhancement of radiation response of prostatic carcinoma by taxol: therapeutic potential for late-stage malignancy. *Anticancer Res* 15: 93–98

Maeda H, Matsumura Y (1989) Tumoritropic and lymphotropic principles of macromolecular drugs. *Crit Rev Ther Drug Carrier Syst* 6: 193–210

Mason KA, Milas L, Peters LJ (1995) Effect of paclitaxel (taxol) alone and in combination with radiation on the gastrointestinal mucosa. *Int J Radiat Oncol Biol Phys* 32: 1381–1389

Matsumura Y, Maeda H (1986) A new concept for macromolecular therapeutics in cancer chemotherapy: mechanism of tumoritropic accumulation of proteins and the antitumor agent smancs. *Cancer Res* 46: 6387–6392

Milas L, Hunter NR, Mason KA, Kurdoglu B, Peters LJ (1994) Enhancement of tumour radioresponse of a murine mammary carcinoma by paclitaxel. *Cancer Res* 54: 3506–3510

Milas L, Hunter NR, Mason KA, Milross CG, Saito Y, Peters LJ (1995) Role of reoxygenation in induction of enhancement of tumour radioresponse by paclitaxel. *Cancer Res* 55: 3564–3568

Morton RF, Jett JR, McGinnis WL, Earle JD, Therneau TM, Krook JE, Elliott TE, Mailliard JA, Nelimark RA, Maksymiuk AW (1991) Thoracic radiation therapy alone compared with combined chemoradiotherapy for locally unresectable non-small cell lung cancer. A randomized, phase III trial. *Ann Intern Med* 115: 681–686

Penney DP, Rubin P (1977) Specific early fine structural changes in the lung irradiation. *Int J Radiat Oncol Biol Phys* 2: 1123–1132

Rodriguez M, Sevin BU, Perras J, Nguyen HN, Pham C, Steren AJ, Koechli OR, Averette HE (1995) Paclitaxel: a radiation sensitizer of human cervical cancer cells. *Gynecol Oncol* 57: 165–169

Rowinsky EK, Chaudhry V, Forastiere AA, Sartorius SE, Ettinger DS, Grochow LB, Lubejko BG, Cornblath DR, Donehower RC (1993) Phase I and pharmacologic study of paclitaxel and cisplatin with granulocyte colony-stimulating factor: neuromuscular toxicity is dose-limiting. *J Clin Oncol* 11: 2010–2020

Rowinsky EK, Donehower RC (1995) Paclitaxel (taxol). *N Engl J Med* 332: 1004–1014

Sause W, Kolesar P, Taylor SI, Johnson D, Livingston R, Komaki R, Emami B, Curran Jr W, Byhardt R, Dar AR, Turrisi III A (2000) Final results of phase III trial in regionally advanced unresectable non-small cell lung cancer: Radiation Therapy Oncology Group, Eastern Cooperative Oncology Group, and Southwest Oncology Group. *Chest* 117: 358–364

Sinclair WK, Morton RA (1966) X-ray sensitivity during the cell generation cycle of cultured Chinese hamster cells. *Radiat Res* 29: 450–474

Taghian AG, Assaad SI, Niemierko A, Kuter I, Younger J, Schoenthaler R, Roche M, Powell SN (2001) Risk of pneumonitis in breast cancer patients treated with radiation therapy and combination chemotherapy with paclitaxel. *J Natl Cancer Inst* 93: 1806–1811

Terasima T, Tolmach LJ (1963) X-ray sensitivity and DNA synthesis in synchronous populations of HeLa cells. *Science* 140: 490–492

Tishler RB, Geard CR, Hall EJ, Schiff PB (1992) Taxol sensitizes human astrocytoma cells to radiation. *Cancer Res* 52: 3495–3497

Uchino H, Matsumura Y, Negishi T, Koizumi F, Hayashi T, Honda T, Nishiyama N, Kataoka K, Naito S, Kakizoe T (2005) Cisplatin-incorporating polymeric micelles (NC-6004) can reduce nephrotoxicity and neurotoxicity of cisplatin in rats. *Br J Cancer* 93: 678–687

Weiss RB, Donehower RC, Wiernik PH, Ohnuma T, Gralla RJ, Trump DL, Baker Jr JR, Van Echo DA, Von Hoff DD, Leyland-Jones B (1990) Hypersensitivity reactions from taxol. *J Clin Oncol* 8: 1263–1268

Yu TK, Whitman GJ, Thames HD, Strom E, McNeese MD, Perkins GH, Schechter N, Kau S, Buzdar AU, Hortobagyi GN, Thomas E, Buchholz TA (2003) Clinically-relevant pneumonitis is not increased in breast cancer patients treated with sequential paclitaxel and radiation. *Int J Radiat Oncol Biol Phys* 57(2 Suppl): S127–S128

Yu TK, Whitman GJ, Thames HD, Buzdar AU, Strom EA, Perkins GH, Schechter NR, McNeese MD, Kau SW, Thomas ES, Hortobagyi GN, Buchholz TA (2004) Clinically relevant pneumonitis after sequential paclitaxel-based chemotherapy and radiotherapy in breast cancer patients. *J Natl Cancer Inst* 96: 1676–1681

VOLUME 123, NO. 1, 18 OCTOBER 2007

ISSN: 0168-3659

ELSEVIER

journal of controlled release

OFFICIAL JOURNAL OF THE CONTROLLED RELEASE SOCIETY
AND THE JAPANESE SOCIETY OF DRUG DELIVERY SYSTEM

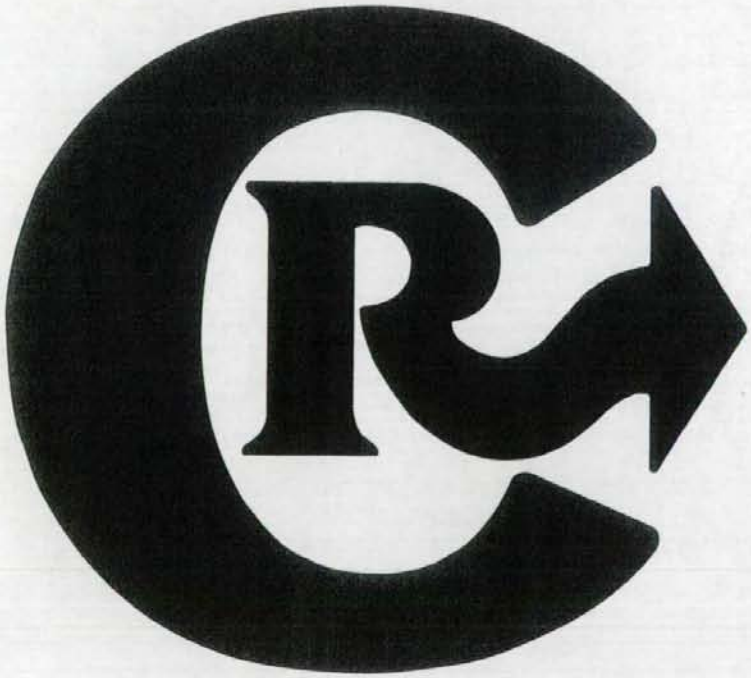

Available online at www.sciencedirect.com
ScienceDirect
Journal of Controlled Release 123 (2007) 11–18
journal of controlled release
www.elsevier.com/locate/jconrel

What are determining factors for stable drug incorporation into polymeric micelle carriers? Consideration on physical and chemical characters of the micelle inner core

Tatsuhiro Yamamoto [a], Masayuki Yokoyama [a,*], Praneet Opanasopit [a,b], Akihiro Hayama [c], Kumi Kawano [c], Yoshie Maitani [c]

[a] *Yokoyama Project, Kanagawa Academy of Science and Technology, KSP East 404, Sakado 3-2-1, Takatsu-ku, Kawasaki, Kanagawa 213-0012, Japan*
[b] *Department of Pharmaceutical Technology, Faculty of Pharmacy, Silpakorn University, Nakhonpathom, 73000, Thailand*
[c] *Institute of Medicinal Chemistry, Hoshi University, 2-4-41 Ebara, Shinagawa, Tokyo 142-8501, Japan*

Received 9 May 2007; accepted 24 July 2007
Available online 29 July 2007

Abstract

Partially benzyl-esterified poly(ethylene glycol)-*b*-poly(aspartic acid) (PEG-P(Asp(Bzl))) having different hydrophobic inner-core structure were synthesized and analyzed. We obtained two types of the block copolymers for formation of polymeric micelle drug carriers; one had an amide-bond ratio of 1:3 (α/β) in the poly(aspartic acid) residues through alkaline hydrolysis, and the other one had 100% of the α-amide through acid hydrolysis. Subsequently, we prepared partially benzyl-esterified block copolymers with an esterification degree of 40 to 100% in the aspartic acid residue. Regarding camptothecin (CPT) incorporation into polymeric micelles, we evaluated effects that block copolymers' inner hydrophobic block structures have on CPT behavior. Regarding CPT-incorporation stability, PEG-P(α,β-Asp(Bzl) block copolymers with the α and β-amides were found to exhibit higher CPT-incorporation stability. Using fluorescent probes, we evaluated the properties of inner-core blocks such as hydrophobicity and mobility/rigidity, and the findings implied that stable CPT incorporation could be obtained by an adequate balance between the micelle inner core's hydrophobicity and the micelle inner core's rigidity or between the micelle inner core's hydrophobicity and steric configuration of the hydrophobic block chain.

Keywords: Polymeric micelle; Camptothecin; Incorporation; Inner core; Hydrophobicity

1. Introduction

Polymeric micelles have attracted much attention as a nano-sized drug carrier in drug delivery system (DDS) owing to their advantages such as very small size in a range of 10–100 nm and high structural stability [1–4]. The enhanced permeability and retention (EPR) effect [5,6] enables polymeric micelles to deliver various drugs selectively to solid tumor sites. For a successful achievement of this tumor targeting, stable drug incorporation into the inner core of the micelle is very important. In general, for targeting by intravenous injection, the targeting is unsuccessful if the drug-incorporation stability is low. Owing to low incorporation stability, a drug is too quickly released from the carrier, resulting in non-specific supply of drug in the bloodstream. Especially for the EPR mechanism's tumor targeting, stability is essential because effective targeting needs a considerably long period (e.g., 10 to 48 h) in which to function. Recently, a large number of studies on polymeric-micelle carriers have appeared; however, only a limited number of studies succeeded in tumor targeting *in vivo* [7,8]. It is expected that one reason for the unsuccessful targeting is unstable drug incorporation in *in vivo* circumstances, since targeting is unsuccessful if most drug is released before the carrier system reaches the target. The other important factor related to drug incorporation into polymeric micelles is efficiency. High drug-incorporation efficiency is preferable both in basic research and in clinical developments.

* Corresponding author. Tel.: +81 44 819 2093; fax: +81 44 819 2095.
E-mail address: yokoyama2093ryo@ksp.or.jp (M. Yokoyama).

0168-3659/$ - see front matter © 2007 Elsevier B.V. All rights reserved.
doi:10.1016/j.jconrel.2007.07.008

The first successful example of the tumor targeting with a polymeric micelle carrier was adriamycin-incorporated polymeric micelle system [8,9]. In this system, pharmacologically active adriamycin was physically incorporated into the micelle's hydrophobic inner core, which formed from the adriamycin-conjugated poly(aspartic acid) polymer blocks. The stable drug incorporation was achieved by a high concentration of the total adriamycin molecules (both the chemically conjugated ones and the physically entrapped ones) in the micelle inner core. This study suggested that not only hydrophobic interactions but also $\pi-\pi$ interactions were important for the stable incorporation because the adriamycin molecules are rich in π-electrons. This adriamycin system is considered to be in a special case owing to the use of the chemically conjugated drug molecules as the source of cohesive interactions for drug incorporation as well as for micelle formation. In order to develop a more universal methodology that can be applied for various drugs, we have developed polymeric micelle systems that do not use drug molecules as the micelle's hydrophobicity source. For this type of the polymeric micelle system, we have reported polymeric micelles containing KRN-5500 [10] and camptothecin [11–13].

In the previous report, we reported successful incorporation of camptothecin (CPT) into polymeric carriers that did not use CPT molecules as the micelle's hydrophobicity source. CPT is a water-insoluble antitumor chemical whose action mechanism is inhibition of DNA topoisomerase I [14]. Its clinical trial failed because of a strong side effect at the bladder; however its two derivatives (CPT-11 and Topotecan) were approved in 1990s. This fact indicates the high potency of CPT and CPT derivatives as anticancer drugs. If CPT and CPT derivatives can facilitate tumor targeting, a great contribution to the cancer chemotherapy is feasible. We achieved stable drug incorporation, long circulation in the bloodstream, and a considerably high level of tumor targeting by optimizing the inner-core-forming block of the PEG-P(aspartate) block copolymer [11–13]. In this optimized block copolymer, the benzyl group was introduced in ca. seventy molar percent of the aspartic acid residue; the benzyl group functioned as the hydrophobic source of the micelle inner core. With regard to drug targeting, this benzyl ester content (60 to 70%) proved to be the best; both drug-incorporation stability and targeting efficiency were lowered in the case of the lower benzyl content and in the case of the higher (100%) benzyl content. This is very interesting because the more-hydrophobic polymer block (the 100%-benzyl-content case) was unfavorable irrespective of the fact that hydrophobic interactions are a main cohesive interaction working both for micelle formation and for drug incorporation.

In this paper, we analyze the effects that the chemical structures of the inner core-forming hydrophobic block have on CPT incorporation, and we focus on aspects other than hydrophobic interactions. Through this analysis, we will establish a strategy to design block copolymers that enable anticancer drugs to efficiently target tumors. For this purpose, we prepared two types of PEG-P(aspartate) block copolymers; one whose aspartate amide bond was a mixture of α-and β-types and the other one whose amide bond consisted only of the α-type. Using fluorescent probes, we measured properties of the inner core, hydrophobicity, and mobility/rigidity, and we analyzed these results in relation to drug-incorporation efficiency and drug-incorporation stability.

2. Materials and methods

2.1. Materials

(s)-(+)-Camptothecin was purchased from Aldrich Chem. Co. (Milw., WI, USA). Poly(ethylene glycol)-*b*-poly(β-benzyl L-aspartate) (PEG-PBLA) was synthesized, as reported previously [15]. Trifluoromethanesulfonic acid (TFMSA) and 1,8-diazabicyclo[5.4.0]undec-7-ene (DBU) were purchased from Wako Pure Chemical (Tokyo, Japan). Thioanisole and m-cresol were purchased from Tokyo Kasei Kogyo Co. Ltd. (Tokyo, Japan). 1,3-Bis(1-pyrenyl)propane (dipyrene) was purchased from Dojindo Laboratories (Kumamoto, Japan). Other chemicals were of reagent grade.

2.2. Synthesis of partially benzyl-esterified poly(ethylene glycol)-b-poly(aspartic acid) (PEG-P(Asp(Bzl)))

As shown in Scheme 1, we synthesized partially benzyl-esterified poly(ethylene glycol)-*b*-poly(aspartic acid) with two types of the poly(aspartic acid) block. First, we hydrolyzed the poly(ethylene glycol)-*b*-poly(β-benzyl L-aspartate) (PEG-PBLA) by using two methods that brought about two types of the poly(aspartic acid) block in the block polymers: the first method was alkaline hydrolysis, which yielded the α-amide and β-amide mixture type; and the second method was acid hydrolysis, which yielded the α-amide pure type. On the second step, we formed benzyl ester at the aspartic acid residues of the PEG-P(Asp) block copolymers.

2.2.1. Synthesis of poly(ethylene glycol)-b-poly(β-benzyl L-aspartate)(PEG-PBLA)

We synthesized poly(ethylene glycol)-*b*-poly(β-benzyl L-aspartate) (PEG-PBLA) by ring-opening polymerization of β-benzyl L-aspartate *N*-carboxy anhydride (BLA-NCA) from the

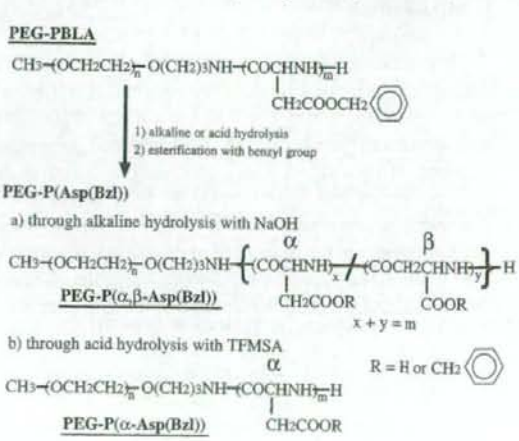

Scheme 1. Synthetic scheme of two different amide bond types of block copolymers.

terminal primary amino group of α-methyl-ω-aminopropoxy poly(ethylene glycol), as reported previously [15]. We use a codename indicating a molecular weight of the poly(ethylene glycol) block and the unit number of the poly(amino acid) block. For example, 5-27 PEG-PBLA indicates that the molecular weight of the PEG block is 5000, and the unit number of the Asp residue in the PBLA block is 27.

2.2.2. Synthesis of poly(ethylene glycol)-b-poly(aspartic acid) (PEG-P(Asp))

We removed the benzyl ester protecting group from PEG-PBLA to obtain poly(ethylene glycol)-*b*-poly(aspartic acid) block copolymers. To carry out this debenzylation, we used the following two methods: (1) alkaline hydrolysis with NaOH and (2) acid hydrolysis with TFMSA [16,17]. Conducting a ^{1}H NMR analysis, we observed no benzyl group in the products obtained by either of the two hydrolysis methods.

2.2.2.1. Alkaline hydrolysis of the PEG-PBLA block copolymer. We deprotected the benzyl ester by conducting alkaline hydrolysis that featured NaOH. To 3.97 g of 5–27 PEG-PBLA, we added a 0.5 N NaOH aqueous solution (30.0 mL, 1.5 equivalent mol. with respect to the aspartic acid group). The reaction mixture was stirred at room temperature for 2 h. The solution became transparent during this period. Then, we added 6 N HCl (10 equivalent mol. to the Asp unit) to the solution, which we purified by performing dialysis. To this end, we used a Spectra/Por 6 dialysis membrane (molecular weight cut-off is 1000) in water, followed by lyophilization. We obtained as white powder the poly(ethylene glycol)-*b*-poly(aspartic acid) (PEG-P(Asp)). To determine the ratio between the α-amide and the β-amide of the aspartic acid unit, we used ^{1}H NMR spectroscopy (methine proton of the α-amide at 4.68 ppm and methine proton of the β-amide at 4.47 ppm in D_2O at alkaline pH (adjusted with NaOD) [18].

2.2.2.2. Acid hydrolysis of the PEG-PBLA block copolymer. Alternatively, we subjected PEG-PBLA to acid hydrolysis by using trifluoromethanesulfonic acid (TFMSA) [16,17]. We dissolved PEG-PBLA (3.02 g) in 53 mL of trifluoroacetic acid (TFA), and then, we added 8.9 mL of thioanisole, 8.0 mL of m-cresol, and 6.6 mL of trifluoromethanesulfonic acid (TFMSA) to the solution, which was in an ice bath. The reaction mixture was stirred at 0 °C for 2 h. The color of the reaction mixture became green. To achieve reprecipitation, we poured the solution dropwise into 1500 mL of diethylether at 0 °C. The precipitate was collected and dried. The obtained precipitate was dissolved in dimethyl sulfoxide (DMSO), and the solution was dialyzed (we used a Spectra/Por 6 dialysis membrane, and the molecular weight cut-off was 1000) against water. We then performed lyophilization. To determine the purity of the α-amide form of the Asp unit, we used ^{1}H NMR spectroscopy in the same way as that for the alkaline hydrolysis stated above.

2.3. Esterification of PEG-P(Asp) with benzyl group

For the esterification of the PEG-P(Asp) block copolymer with the benzyl group, we used a nucleophilic-substitution reaction that occurred between benzyl bromide and carboxyl groups of the Asp block, as reported previously [11]. We dissolved PEG-P(Asp) in DMF. Then, we added benzyl bromide and DBU to the solution at various molar ratios both of benzyl bromide and DBU to the Asp unit, as summarized in Table 1. The reaction mixture was stirred at 50 °C for 16 h. The solution was added dropwise to diethylether at 0 °C, and then the precipitate was collected and dried. The obtained precipitate was dissolved in DMSO, and 6 N HCl (a molar equivalent to the molar of DBU) was added to the solution. The solution was dialyzed (a Spectra/Por 6 dialysis membrane was used), molecular weight cut-off was 1000) against water. We then performed lyophilization. To analyze the obtained block copolymers, we used ^{1}H NMR spectroscopy in DMSO-d_6 containing 3 v/v% trifluoroacetic acid. To determine the content of the benzyl group of the polymers, we identified a peak area ratio between the methylene protons of the benzyl group and the methylene protons of the PEG block. Table 1 lists the benzyl ester content of the block copolymers.

2.4. Incorporation of CPT into polymeric micelles

We incorporated the CPT into polymeric micelles by performing an evaporation method as reported previously

Table 1
Esterification conditions of PEG-P(Asp) block copolymers

Code	In feed						Obtained	
	Block copolymer		Benzyl bromide		DBU		Yield (mg)	Benzyl ester content per Asp unit
	Weight (mg)	Asp (mmol)	Weight (mn)	Molar ratio to Asp	Weight (mg)	Molar ratio to Asp		
PEG-P(α,β-Asp(Bzl 84%))	224.2	0.70	239.6	2.00	192.1	1.80	255.6	84%
PEG-P(α,β-Asp(Bzl 61%))	505.5	1.58	270.2	1.00	240.0	1.00	521.2	61%
PEG-P(α,β-Asp(Bzl 50%))	507.9	1.59	217.5	0.80	193.0	0.80	535.5	50%
PEG-PBLA	–	–	–	–	–	–	–	100%
PEG-P(α-Asp(Bzl 63%))	504.6	1.57	269.2	1.00	238.7	1.00	480.5	63%
PEG-P(α-Asp(Bzl 55%))	210.8	0.66	73.2	0.65	65.7	0.65	193.3	55%
PEG-P(α-Asp(Bzl 41%))	219.0	0.68	59.4	0.51	51.8	0.51	193.0	41%

[19]. A block copolymer and CPT were dissolved in a mixture of chloroform and acetonitrile (3:2, v/v) at various CPT-to-polymer weight ratios, then the solution was stirred at ca 40 °C under a nitrogen gas flow. The solvent was completely evaporated, and water (3 mL) was added to the residue. Then, we sonicated the solution by using a probe-type sonicator (vibra-cell VCX-750, Sonics & Materials Inc., Connecticut, USA) at 80 °C for 2 min in a cycle of sonication for 0.5 sec and standby for 1.0 sec. The solution was filtered through a 1 μm filter (Puradisc 25NYL, Whatman, USA). The polymeric micelle incorporating CPT was obtained in this filtrate.

2.5. Characerization of CPT-incorporated polymeric micelles

Our task, now, was to determine the amount of CPT that was incorporated into the polymeric micelles. Using a UV–Vis spectrometer (V-550 UV–Vis spectrometer, Jasco, Tokyo, Japan), we performed an absorbance measurement at 370 nm in a mixture of DMSO and water (9:1, v/v).

We evaluated the incorporation stability of the CPT in the polymeric micelles by performing gel-permeation chromatography, for which we used an HPLC system (LC-2000 series, Jasco, Tokyo, Japan) equipped with a TSK-gel G4000 PW_{XL} column. Water functioned as an eluent at a flow rate of 1.0 mL/min at 40 °C. We detected CPT by measuring absorbance at 351 nm [11]. We evaluated the stability by using a peak area of the CPT-incorporated micelle. We obtained a ratio of the CPT peak area/CPT concentration. We judged that the stability was higher when this ratio was larger.

2.6. Evaluation of inner core hydrophobicity and mobility/rigidity

We then set out to determine two things: first, the hydrophobicity of the polymeric micelles' inner core and, second, a critical micelle concentration of block copolymers. To make these determinations, we used fluorescence spectroscopy (FP-6500, Jasco, Tokyo, Japan) and used pyrene as a fluorescent probe. We used the evaporation method to prepare the polymeric micelles, and concentrations of their aqueous solutions varied from 0.03 μg/mL to 5 mg/mL. We added 5 μL of a pyrene solution in acetone to the 4 mL of the polymeric-micelle solution; then, we evaporated the acetone by stirring the solution overnight at room temperature while the concentration of pyrene was 6.0×10^{-7} M. The measured wavelength of emission was fixed at 383 nm, and band widths of both excitation and emission were 5 nm. Excitation spectra were recorded at micelle concentrations ranging from 0.03 μg/mL to 5 mg/mL. To determine the critical micelle concentration (CMC), we plotted the ratios of the excitation spectra's fluorescent intensities at 339 nm and 334 nm (I_{339}/I_{334}). This fluorescent intensity ratio was also used as a parameter indicating the hydrophobicity of the inner core at a high concentration (2 mg/mL) of block copolymers. This concentration was much greater than CMCs of the micelles.

We evaluated the mobility/rigidity of the polymeric micelles' inner core by using fluorescence spectroscopy of 1,3-bis(1-pyrenyl)propane (dipyrene) in the same experimental protocol as that for pyrene. For the fluorescent measurements with dipyrene, a concentration of dipyrene was 2.2×10^{-7} M. The wavelength of excitation was fixed at 333 nm. The band widths of both excitation and emission were 5 nm. From the emission spectra, we measured fluorescent intensity ratios between 480 nm (excimer complex) and 398 nm (pyrene monomer) when a polymer concentration was 2 mg/mL.

3. Results and discussion

3.1. Synthesis of partially benzylated PEG-P(Asp) block copolymers

Poly(ethylene glycol)-*b*-poly(aspartic acid) (PEG-P(Asp)) containing different amide-bonds in the P(Asp) block were successfully synthesized. For structures of copolymers see Scheme 1. We obtained two different PEG-P(Asp) block copolymers through two hydrolysis methods, alkaline hydrolysis and acid hydrolysis.

The alkaline hydrolysis with sodium hydroxide brought about the PEG-P(Asp) block copolymer whose amide-bonds were a mixture of the α-amide and the β-amide. It is known that α-amide bonds of the PBLA block converted to β-amide bonds in an alkaline hydrolysis procedure [18]. We found that the ratio of the α-amide and the β-amide was 25:75 (α/β) by analyzing ^{1}H NMR spectrum in D_2O. We successfully removed the benzyl ester protecting group from 5–27 PEG-PBLA block copolymer. The complete deprotection was proven by the absence of the benzyl proton peaks in a ^{1}H NMR spectrum (data not shown).

We performed the acid hydrolysis on the 5–27 PEG-PBLA block copolymer by using TFMSA. By doing this, we obtained the PEG-P(Asp) block copolymer where the PBLA block completely retained the α-amide structure. We obtained the PEG-P(Asp) block copolymer whose amide bonds were composed of 100% of the α-amide. We confirmed this α-amide purity by measuring a ^{1}H NMR spectrum in D_2O.

We performed partial esterification of the copolymers' P(Asp) block. The esterification was successfully achieved for both the two types of PEG-P(Asp) block copolymers obtained through the alkaline hydrolysis and the acid hydrolysis. We successfully controlled the content of the P(Asp) block's benzyl group. The benzyl group content ranged from 40 to 80%. To control the benzyl group content, we varied molar ratios both of benzyl bromide and of DBU to the Asp units. Consequently, we obtained two types of block copolymers having different amide-bonds, PEG-P(α,β-Asp(Bzl)) and PEG-P(α-Asp(Bzl)). To determine the contents of the block copolymers' benzyl group, we used ^{1}H NMR spectroscopy by using DMSO-d_6 containing 3 v/v% trifluoroacetic acid as a solvent. Table 1 summarizes these results of the block copolymer syntheses.

3.2. Incorporation efficiency and stability of camptothecin (CPT) into polymeric micelles

We incorporated camptothecin (CPT) into polymeric micelles. To do this, we used an evaporation method and varied the weight ratios of CPT to the block copolymers (5, 10, 20 and

40 wt.%). Fig. 1a shows plots of CPT incorporation efficiency against CPT/polymer weight ratios. With the exception of a few plot points, all block copolymers clearly exhibited a reduction in the incorporation efficiency where there was an increase in the CPT/polymer ratio. This behavior may be due to the capacity limit of the hydrophobic inner core for drug incorporation. Even with this capacity limit, the micelle's drug contents were very high. For PEG-P(α-Asp(Bzl 55%)) at 40 wt.% of the CPT/polymer ratio, the drug content in the micelle was 25 wt.%. This value is high, and we calculated it by assuming that there was no loss of the block copolymer throughout the incorporation process. When we examined differences of the incorporation efficiency between the α and β-amide mixture type and the α-amide pure type, we observed no clear tendency. Fig. 1b illustrates this observation by showing the plots of the 10 wt.% of the CPT/polymer ratio.

In contrast, we observed pronounced and interesting differences in incorporation-stability between the two types of block copolymers. Fig. 2a shows the CPT-incorporation stability evaluated by using gel-permeation chromatography (GPC). In this aqueous GPC analysis, the stably incorporated CPT in the polymeric micelles can elute at a gel-exclusion

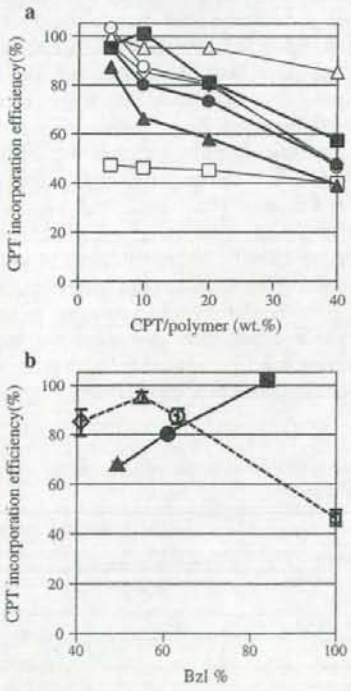

Fig. 1. Incorporation efficiency of CPT-incorporated polymeric micelles. Polymeric micelles form from α-amide and β-amide mixture type block copolymer, PEG-P(α,β-Asp(Bzl)) (■: Bzl 84%, ●: Bzl 61%, ▲: Bzl 50%) and α-amide type block copolymer, PEG-P(α-Asp(Bzl)) (□: Bzl 100% (PEG-PBLA), ○: Bzl 63%, △: Bzl 55%, ◇: Bzl 41%). Incorporation efficiencies are plotted as a function of a) weight ratios of CPT to the block copolymers in feed and b) benzyl (Bzl) contents at 10 wt.% of the CPT weight ratio to the block copolymer. Solid line: PEG-P(α,β-Asp(Bzl)), and dotted line: PEG-P(α-Asp (Bzl)). Data are plotted by the mean ± standard deviation of two experiments (b).

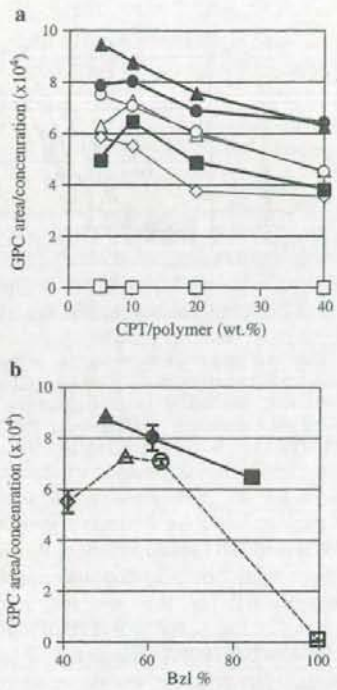

Fig. 2. Incorporation stability of CPT-incorporated polymeric micelles. Polymeric micelles form from α-amide and β-amide mixture type block copolymer, PEG-P(α,β-Asp(Bzl)) (■: Bzl 84%, ●: Bzl 61%, ▲: Bzl 50%) and α-amide type block copolymer, PEG-P(α-Asp(Bzl)) (□: Bzl 100% (PEG-PBLA), ○: Bzl 63%, △: Bzl 55%, ◇: Bzl 41%). The stability is evaluated by peak area of CPT-incorporated micelle normalized by the CPT concentration. Data are plotted as a function of a) weight ratios of CPT to the block copolymers, or b) as a function of benzyl (Bzl) contents at 10 wt.% of the CPT to the block copolymer. Solid line: PEG-P(α,β-Asp(Bzl)), and dotted line: PEG-P(α-Asp (Bzl)). Data are plotted by the mean ± standard deviation of two experiments (b).

volume that is the elution position of the micelles while unincorporated CPT and unstably incorporated CPT adhere to the GPC column by undergoing hydrophobic interactions. Therefore, we found that the incorporation stability was higher when there was a higher peak-area/CPT-concentration ratio. In fact, we reported that these ratios' increases closely related to enhancement in *in vivo* anti-cancer activity for an adriamycin-incorporated polymeric micelle system [20,21]. As Fig. 2a shows, the PEG-P (α,β-Asp(Bzl)) block copolymers that featured the α and β-amides exhibited higher CPT incorporation stability than did the corresponding block copolymers that featured the α-amide. PEG-P(α,β-Asp(Bzl 61% and 50%)) exhibited higher GPC-Area/CPT-concentration values than did PEG-P(α-Asp(Bzl 63%, 50% and 41%)) in all the CPT/polymer weight ratios from 5 to 40%. Both α-amide and β-amide are isomers. Therefore, in general, the two isomers do not differ from each other in terms of physical properties such as hydrophobicity. Therefore, the observed stability differences between the two isomer types suggest that steric configuration or physical factors other than hydrophobicity influenced the CPT-incorporation stability. Interestingly, the block copolymers

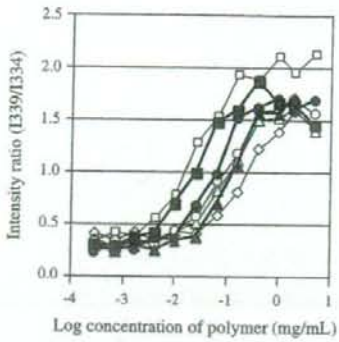

Fig. 3. Fluorescent intensity ratio of I_{339}/I_{334} of pyrene as a function of logarithmic concentrations of block copolymers. The α-amide and β-amide mixture type block copolymer, PEG-P(α,β-Asp(Bzl)) (◆, Bzl 84%; ■, Bzl 61%; ▲, Bzl 50%) and α-amide type block copolymer, PEG-P(α-Asp(Bzl)) (◇, Bzl 100% (PEG-PBLA); □, Bzl 63%; △, Bzl 55%; ○, Bzl 41%) are plotted.

PEG-P(α,β-Asp(Bzl 84%) and PEG-P(α-Asp (Bzl 100%)), which were significantly hydrophobic, exhibited lower CPT-incorporation stability than did the corresponding block copolymers that had lower benzyl (Bzl) content. In particular, PEG-P (α-Asp(Bzl 100%) exhibited quite low stability values, even though this polymer was the most hydrophobic block copolymer. The above-stated behavior is clearer in the plots for 10 wt.% of the CPT/polymer ratio, as shown in Fig. 2b.

These results indicate that the CPT-incorporation stability is governed not only by hydrophobicity but also by other factors such as steric configuration and/or mobility/rigidity of the block polymer, even though hydrophobic interactions are the main adhesive force both for micelle formation and drug incorporation.

3.3. Fluorescent measurements of the polymeric micelle inner cores in relation to stable drug incorporation

We conducted fluorescent measurements of the micelle's inner core. Pyrene and dipyrene were incorporated into the polymeric micelles' inner cores. The purpose of our measurements was to evaluate two inner-core properties: hydrophobicity and mobility/rigidity, by the use of pyrene and dipyrene, respectively.

Pyrene is known to exhibit a peak shift in its excitation spectrum upon its incorporation into a hydrophobic inner-core [22]. Fig. 3 plots the fluorescent intensity ratios of I_{339}/I_{334} in excitation spectra. We determined the critical micelle concentration (CMC) of block copolymers. (Table 2) In two amide-types of block copolymers, PEG-P(α,β-Asp(Bzl) and PEG-P (α-Asp(Bzl)), CMC values gradually increased on a range from 4 μg/mL to 39 μg/mL, as the benzyl content decreased. We examined the most hydrophobic block copolymers in each amide-type block copolymer — PEG-PBLA (=PEG-P(α-Asp (Bzl 100%)) and PEG-P(α,β-Asp(Bzl 84%)). These copolymers' CMC values were the smallest of all: the 4 and 5 μg/mL, respectively.

To evaluate the inner core's hydrophobicity, we measured the fluorescent intensity ratios of I_{339}/I_{334}. These measurements were conducted at 2 mg/mL of the polymer concentration. This polymer concentration was much greater than CMC values of all the polymers. The larger values of the ratios indicate the more-hydrophobic inner cores. The most hydrophobic block copolymer, PEG-PBLA, exhibited a value (2.0) that was slightly higher than those of the others, while the other block copolymers exhibited similar values (1.6–1.7) irrespective of their various benzyl contents. These results imply that small amounts of pyrene probes did not reveal the total potential hydrophobicity of the micelle inner core, probably because pyrene probes were present in small sites where hydrophobic benzyl groups associated in the polymeric micelle core.

We also evaluated the mobility/rigidity of the polymeric micelles' inner core by using a fluorescent probe, dipyrene. Dipyrene forms an intramolecular excimer complex if the atmosphere surrounding the probe has low rigidity [23]. Therefore, when the inner-core mobility increases, the value of fluorescent intensity ratio between excimer complex and monomer increases. Table 2 summarizes fluorescent intensity ratios of I_{480}/I_{398}. All measurements were conducted at 2 mg/mL of the polymer concentration. This polymer concentration was much greater than CMC values of the polymers.

PEG-P(α-Asp(Bzl 100%)), PEG-PBLA, exhibited the lowest I_{480}/I_{398} value, 0.04. This value indicates that PEG-PBLA had the most rigid inner core. This block copolymer, however, did not exhibit stable drug incorporation at all, as shown in Fig. 2. The low stability indicates that PEG-PBLA did not obtain stable drug incorporation simply owing to the micelle inner core's rigidity. The α-amide and β-amide mixture type of block copolymesr, PEG-P(α,β-Asp(Bzl 50, 61 and 84%)), exhibited significantly lower values (0.10 to 0.11) than those (0.22 to 0.41) of the α-amide pure type polymers, PEG-P(α-Asp (Bzl 41%, 50% and 61%)). According to our findings, the former block copolymers that exhibited the greatest drug incorporation stability possessed more rigid inner cores than the corresponding later block copolymers.

Table 2
Evaluation of CMC and inner core properties by the use of fluorescent probes pyrene and dipyrene

Code	CMC (μg/mL)[a]	I339/I334 of pyrene excitation[b]	I480/I398 of dipyrene emission[b]
PEG-P(α,β-Asp (Bzl 84%))	5	1.7	0.10
PEG-P(α,β-Asp (Bzl 61%))	13	1.6	0.11
PEG-P(α,β-Asp (Bzl 50%))	28	1.7	0.10
PEG-PBLA	4	2.0	0.04
PEG-P(α-Asp (Bzl 63%))	15	1.7	0.41
PEG-P(α-Asp (Bzl 55%))	18	1.6	0.23
PEG-P(α-Asp (Bzl 41%))	39	1.6	0.22

[a] Obtained from Fig. 3 plot with pyrene.
[b] At 2 mg/mL of polymer.

The above-stated results imply that stable CPT incorporation derived from an adequate balance between micelle inner cores' hydrophobicity and micelle inner cores' rigidity. Alternatively, steric configuration of the inner core-forming polymer chain would be another factor that controls stability. This is so because the α- and β-amide mixture type block copolymers have one additional alkyl methylene chain (CH_2) in the β-amide unit in comparison with the α-amide chain. Accordingly, the α- and β-amide mixture type block copolymer can sandwich a hydrophobic drug molecule between two benzyl groups in a more favorable and stable manner than the α-amide pure type block copolymer.

In this paper, we reveal that hydrophobicity is not the single factor controlling the CPT-incorporation stability into the micelle inner core. In other words, other factor(s) over hydrophobicity can contribute to CPT-incorporation stability. We could not elucidate the other controlling factor(s), even though both the rigidity of the inner core and the steric configuration of the micelle-forming block's main chain were possible factors responsible for the stable incorporation.

Through its tumor-targeting effect, the adriamycin-incorporated polymeric-micelle system substantially enhanced *in vivo* antitumor activity. Concerning this system, we suggested that a factor other than hydrophobic properties contributed significantly to stable drug incorporation. And concerning the drug incorporation, the adriamycin-system exhibited the following three distinctive features: (1) two types of drug molecules chemically bound to the inner-core-forming polymer and drug molecules physically entrapped in the inner core arose hydrophobic interactions for micelle formation. (2) The drug content (both chemically bound and physically entrapped) determined the stable drug incorporation that resulted in high tumor-targeting efficiency. (3) The drug-content range in which polymeric micelle formed was very wide. In particular, we obtained a micelle that possessed very large adriamycin content (51 wt.%), and we did so without relying on the formation of a water-insoluble precipitate. (For the CPT case of this paper, the hydrophobic origin for micelle formation was not a drug molecule itself). It is well known that adiriamycin molecules preferentially form a non-covalent dimer complex in aqueous media in a similar manner to that of daunorubicin (an adriamycin analogue) [24]. The main contribution to this dimer formation comes from intermolecular π–π interaction. It is widely believed that the π–π interaction can contribute effectively to stable adriamycin incorporation because this interaction works in a specific manner, like ligand-receptor interactions. The specific interaction is expected to work preferentially for drug incorporation without producing precipitates that can be frequently seen in cases of non-specific hydrophobic interactions. As stated above, the study of the adriamycin micelle system suggested the importance of interactions (other than hydrophobic interaction) for the stable drug incorporation into polymeric micelles. In this paper, we pointed out clear evidence for the presence of stable-drug-incorporation factor(s) other than hydrophobic interactions, even though we could not elucidate the other important factor(s).

Elucidation of the factor(s) is a very important aspect of research on polymeric-micelle carrier systems because stable drug incorporation – in other words, very sustained release from a very small drug reservoir – is required for its drug targeting. It is known that the typical diameter of the hydrophobic inner core ranges from 3 to 10 nm [25,26]. In contrast to this very small size, sustained drug release study has concerned micron-sized carriers in the DDS research history. That is why exceptionally stable drug incorporation is required for polymeric micelle cases. In fact, Kwon et al. reported extremely low diffusion constants of drug molecules, such as 2.0×10^{-19} cm^2/s, in their polymeric micelle system [27]. Elucidation of the controlling factors is important for the establishment of a strategic polymer design in the polymeric micelle drug carrier systems.

4. Conclusion

We synthesized two different types of the block copolymer, PEG-P(α,β-Asp(Bzl)) and PEG-P(α-Asp(Bzl)), and we evaluated the behaviors of camptothecin (CPT) incorporation. For CPT incorporation, the block copolymer whose amide-bond type was a mixture of α-amide and β-amide showed higher CPT-incorporation stability. Furthermore, we used fluorescent probes to measure properties of the inner-core block such as the hydrophobicity and the mobility/rigidity of polymeric micelles. Fluorescent-measurement results imply that stable CPT incorporation could arise from either an adequate balance between hydrophobicity and rigidity or an adequate balance between hydrophobicity and the steric configuration of the polymeric micelle inner core. These results emphasize the high degree to which the exact design of the inner-core block is important for stable drug incorporation that is essential to tumor targeting.

Acknowledgments

This work was supported by Grants-in-Aids from the Ministry of Health, Labour and Welfare of Japan. T. Yamamoto and M. Yokoyama acknowledge support by the Program for Promoting the Establishment of Strategic Research Centers, Special Coordination Funds for Promoting Science and Technology, the Ministry of Education, Culture, Sports, Science, and Technology, Japan.

References

[1] G.S. Kwon, K. Kataoka, Block copolymer micelles as long-circulating drug vehicles, Adv. Drug Deliv. Rev. 16 (1995) 295–301.
[2] G.S. Kwon, T. Okano, Soluble self-assembled block copolymers for drug delivery, Pharm. Res. 16 (1999) 597–600.
[3] M. Yokoyama, in: N. Yui (Ed.), Supramolecular design for biological applications, CRC Press, Boca Raton, 2002, pp. 245–268.
[4] H.M. Aliabadi, A. Lavasanifar, Polymeric micelles for drug delivery, Expert Opin. Drug Deliv. 3 (2006) 139–162.
[5] Y. Matsumura, H. Maeda, A new concept for macromolecular therapeutics in cancer chemotherapy: mechanisms of tumoritropic accumulation of protein and the antitumor agent SMANCS, Cancer Res. 46 (1986) 6387–6392.
[6] H. Maeda, J. Wu, T. Sawa, Y. Matsumura, K. Hori, Tumor vascular permeability and the EPR effect in macromolecular therapeutic, J. Control. Release 65 (2000) 271–284.
[7] H. Uchino, Y. Matsumura, T. Negishi, F. Koizumi, T. Hayashi, T. Honda, N. Nishiyama, K. Kataoka, S. Naito, T. Kakizoe, Cisplatin-incorporating polymeric micelles (NC-6004) can reduce nephrotoxicity and neurotoxicity of cisplatin in rats, Br. J. Cancer 93 (2005) 678–687.

[8] M. Yokoyama, T. Okano, Y. Sakurai, S. Fukushima, K. Okamoto, K. Kataoka, Selective delivery of adriamycin to a solid tumor using a polymeric micelle carrier system, J. Drug Target. 7 (1999) 171–186.
[9] M. Yokoyama, S. Inoue, K. Kataoka, N. Yui, Y. Sakurai, Preparation of adriamycin-conjugated poly(ethylene glycol)-poly(aspartic acid) block copolymer. A new type of polymeric anticancer agent, Makromol. Chem., Rapid Commun. 8 (1987) 431–435.
[10] Y. Matsumura, M. Yokoyama, K. Kataoka, T. Okano, Y. Sakurai, T. Kawaguchi, T. Kakizoe, Reduction of the side effects of an antitumor agent, KRN5500 by incorporation of the drug into polymeric micelles, Jpn. J. Cancer. Res. 90 (1999) 122–128.
[11] P. Opanasopit, M. Yokoyama, M. Watanabe, K. Kawano, Y. Maitani, T. Okano, Block copolymer design for camptothecin incorporation into polymeric micelles for passive tumor targeting, Pharm. Res. 21 (2004) 2001–2008.
[12] M. Watanabe, K. Kawano, M. Yokoyama, P. Opanasopit, T. Okano, Y. Maitani, Preparation of camptothecin-loaded polymeric micelles and evaluation of their incorporation and circulation stability, Int. J. Pharm. 308 (2006) 183–189.
[13] K. Kawano, M. Watanabe, T. Yamamoto, M. Yokoyama, P. Opanasopit, T. Okano, Y. Maitani, Enhanced antitumor effect of camptothecin loaded in long-circulating polymeric micelles, J. Control. Release 112 (2006) 329–332.
[14] V.R. Adams, T.G. Burke (Eds.), Camptothecins in cancer Therapy, Humana Press, Totowa, New jersey, 2005.
[15] M. Yokoyama, G.S. Kwon, T. Okano, Y. Sakurai, T. Seto, K. Kataoka, Preparation of micelle-forming polymer-drug conjugates, Bioconjug. Chem. 3 (1992) 295–301.
[16] H. Arimura, Y. Ohya, T. Ouchi, The formation of biodegradable polymeric micelles from newly synthesized poly(aspartic acid)-block-polylactide AB-Type diblock copolymers, Macromol. Rapid Commun. 25 (2004) 743–747.
[17] H. Arimura, Y. Ohya, T. Ouchi, Formation of core-shell type biodegradable polymeric micelles from amphiphilic poly(aspartic acid)-block-polylactide diblock copolymer, Biomacromolecules 6 (2005) 720–725.
[18] V. Saudek, H. Pivcova, J. Drobnik, NMR study of poly(aspartic acid). II. α-and β-peptide bonds in poly(aspartic acid) prepared by common methods, Biopolymers 20 (1981) 1615–1623.
[19] A. Lavasanifar, J. Samuel, G. S. Kwon. Micelles self-associated from poly (ethylene oxide)-block-poly(*N*-hexyl searate L-aspartamide) by a solvent evaporation method: effect on the solubilization and haemolytic activity of amphotecin B, J. Control. Release 77 (2001) 155–160.
[20] M. Yokoyama, G.S. Kwon, T. Okano, Y. Sakurai, M. Naito, K. Kataoka, Influencing factors on in vitro micelle stability of adriamycin-block copolymer conjugates, J. Control. Release 28 (1–3) (1994) 59–65.
[21] M. Yokoyama, in: G.S. Kwon (Ed.), Polymeric Drug Delivery Systems, Drugs and the Pharmaceutical Science, vol. 148, Taylor & Francis, Boca Raton, FL, 2005, pp. 535–575.
[22] C. Zhao, M.A. Winnik, G. Riess, M.D. Croucher, Fluorescence probe techniques used to study micelle formation in water-soluble block copolymers, Langmuir 6 (1990) 514–516.
[23] H. Dangreau, M. Joniau, M. De Cuyper, I. Hanssens, An intramolecular excimer forming probe used to study the interaction of alpha-lactalbumin with model membranes, Biochem. 21 (1982) 3594–3598.
[24] S.R. Martin, Absorption and circular dichroic spectral studies on the self-association of daunorubicin, Biopolymers 19 (1980) 713–721.
[25] R. Xu, M.A. Winnik, F.R. Hallett, G. Riess, M.D. Croucher, Light-scattering study of the association behavior of styrene-ethylene oxide block copolymers in aqueous solution, Macromolecules 24 (1991) 87–93.
[26] R. Xu, M.A. Winnik, G. Riess, B. Chu, M.D. Croucher, Micellization of polystyrene-poly(ethylene oxide) block copolymers in water. 5. A test of the star and mean-field models, Macromolecules 25 (1992) 644–652.
[27] M.L. Forrest, C.-Y. Won, A.W. Malick, G.S. Kwon, In vitro release of the mTOR inhibitor rapamycin from poly(ethylene glycol)-*b*-poly(ε-caprolactone) micelles, J. Control. Release 110 (2006) 370–377.

Available online at www.sciencedirect.com

ScienceDirect

Reactive & Functional Polymers 67 (2007) 1398–1407

REACTIVE & FUNCTIONAL POLYMERS

www.elsevier.com/locate/react

Thermal modulation of intracellular drug distribution using thermoresponsive polymeric micelles

M. Nakayama [a], J.E. Chung [a], T. Miyazaki [b], M. Yokoyama [a,c], K. Sakai [b], T. Okano [a,*]

[a] *Institute of Advanced Biomedical Engineering and Science, Tokyo Women's Medical University, Kawada-cho 8-1, Shinjuku-ku, Tokyo 162-8666, Japan*

[b] *Department of Applied Chemistry, Waseda University, 3-4-1, Ohkubo, Shinjuku-ku, Tokyo 169-8555, Japan*

[c] *Kanagawa Academy of Science and Technology, Yokoyama "Nano-medical polymers" project, KSP East 404, Sakado 3-2-1, Takatsu-ku, Kawasaki-shi, Kanagawa 213-0012, Japan*

Received 12 June 2007; received in revised form 25 July 2007; accepted 26 July 2007
Available online 9 August 2007

Dedicated to Professor Teiji Tsuruta on the occasion of his 88th birthday (Beiju).

Abstract

Intracellular distribution of free doxorubicin (DOX) or DOX-loaded in polymeric micelles with thermoresponsive outer shells of poly(*N*-isopropylacrylamide) or its copolymers in cultured human breast cancer cells (MCF-7) were investigated by fluorescence and confocal laser scanning microscopy. Free DOX accumulated rapidly and selectively in cell nuclei, independent of temperature changes. In contrast to free drugs, the intracellular distribution of DOX-loaded in the thermoresponsive polymeric micelles was significantly affected by temperature changes across lower critical solution temperature (LCST) of the micelles. Above the micelle LCST, DOX delivered by the micelles was localized uniformly inside of MCF-7 cells. By contrast, the amount of DOX delivered to MCF-7 cells drastically decreased below the micelle LCST due to minimal interaction of the micelles with cell membrane surfaces. These results clearly showed that the mechanism of the intracellular drug localization was different between free drugs and DOX-loaded in the micelles. The thermoresponsive micelles aggressively interacted with the cells and carried DOX into the cells *via* triggered phase transition of the outer shells. In addition, much lower accumulation of free DOX was observed in the resistant cells compared to its parent sensitive MCF-7 due to the resistant mechanism. Of interest, DOX accumulation in the resistant cells was almost in the same level as with MCF-7 (sensitive) cells for the micelle system above the LCST.

Keywords: Poly(*N*-isopropylacrylamide); Thermoresponse; Polymeric micelles; Doxorubicin; Intracellular drug distribution

1. Introduction

Selective anti-cancer drug delivery to solid tumor tissues using drug carriers has been an extremely

* Corresponding author. Tel.: +81 3 3353 8112x30235; fax: +81 3 3359 6046.
E-mail address: tokano@abmes.twmu.ac.jp (T. Okano).

1381-5148/$ - see front matter © 2007 Elsevier Ltd. All rights reserved.
doi:10.1016/j.reactfunctpolym.2007.07.056

attractive application for cancer chemotherapy without severe toxic side effects. For this purpose, several types of drug carriers, such as water-soluble polymers [1,2], liposomes [3,4], and polymeric micelles [5], have been actively investigated.

Amphiphilic block copolymers form core-shell multi-molecular assemblies called polymeric micelles in aqueous media [6,7]. Highly hydrated outer shells of polymeric micelles provide their reliable structural stability in aqueous environments. Hydrophobic inner cores can incorporate a large amount of hydrophobic drug with maintaining their water-solubility due to the presence of the hydrophilic outer shells. Furthermore, nano-ordered diameter range of polymeric micelles (10–200 nm) can allow long circulation in the blood stream avoiding the body's defense systems (reticuloendotherial system, RES) and thus, utilize the enhanced permeability and retention (EPR) effect [8,9] at solid tumor sites for tumor targeting. We have previously reported that polymeric micelles composed of poly(ethylene oxide)-*b*-poly(L-asparate) block copolymers containing an anticancer drug, doxorubicin (DOX), selectively accumulated at solid tumor sites by the passive targeting mechanism, the EPR effect [10,11].

Recently, polymeric micelles with stimuli-responsive drug release mechanisms as a novel concept for anticancer drug delivery have been designed for applications in effective cancer chemotherapy [12–14]. The different drug release kinetics stimulated by physico-chemical signals (e.g., heat, pH, and ultrasound) may lead to maximal cytotoxic action at tumor sites, resulting in locoregional drug accumulation while reducing drug accumulation in normal tissues to inhibit undesirable side effects. These drug carrier systems combining two or more targeting methodologies is defined as multi-targeting systems. In order to accomplish these intelligent drug targeting systems, we have developed polymeric micelles possessing thermoresponsive outer shells [15–17]. Our strategy of cancer chemotherapy using the thermoresponsive polymeric micelles is as follows. Polymeric micelles with drugs circulate in the blood avoiding the RES uptake, and accumulate selectively at solid tumor tissues *via* the EPR-mediated targeting below the micelle LCST. And then the thermoresponsive outer shells of the micelles shrink and change into hydrophobic by local heating at the target sites upon the LCST. This alternation of micelle properties may induce selective drug actions at the heated target site. Simultaneously, this strategy can achieve temporal drug delivery control by local temperature increases.

Poly(*N*-isopropylacrylamide) (PIPAM) is well-known to undergo sharp coil-to-globule transitions at 32 °C in water [18]. This phase transition temperature is called a lower critical solution temperature (LCST). This polymer changes from water-soluble and hydrophilic state (coil) below its LCST to water-insoluble and hydrophobic state (globule: aggregation) above the LCST. Previously, we have already reported successful preparations of thermoresponsive polymeric micelles constructed with two block copolymers, PIPAM-*b*-poly(butyl methacrylate) [15] and PIPAM-*b*-poly(D,L-lactide) [16]. In our previous works, the DOX-loaded thermoresponsive micelles demonstrated successful controlled ON–OFF drug release and subsequent expression of *in vitro* cytotoxicity with applied temperature changes [15,17].

Here, we mainly focus on investigation of intracellular drug delivery and interactions of the thermoresponsive polymeric micelles into/with cultured human breast cancer (MCF-7) cells by fluorescence and laser scanning confocal microscopy in order to understand cytotoxic mechanisms modulated by temperature changes as well as to optimize drug carrier design for the multi-targeting systems.

2. Materials and methods

2.1. Materials

N-Isopropylacrylamide (IPAM) was kindly provided by Kohjin (Japan) and recrystallized from *n*-hexane. D,L-Lactide (LA, TCI, Japan) was purified by recrystallization from ethyl acetate. Butyl methacrylate (BMA, Tokyo Kasei Co. Ltd., Japan), *N*,*N*-dimethylacrylamide (DMAM, Wako Pure Chemicals, Japan) and 3-mercaptopropionic acid (Aldrich) were distilled under reduced pressure. Triethylamine and xylene were purchased from Wako Pure Chemicals and purified by standard methods. Benzoylperoxide (BPO, Kanto Chemical Co., Japan), *N*-ethylacetamide (TCI), *N*,*N*-dimethylacetamide (Wako Pure Chemicals), thionyl chloride (Wako Pure Chemicals), diethyl ether (Wako Pure Chemicals), 2-mercaptoethanol (Wako Pure Chemicals) and tin(II)2-ethylhexanoate (Wako Pure Chemicals) were used as received. Doxorubicin hydrochloride (DOX–HCl) was obtained from Mercian Co., Japan.